Thermodynamic Changes in the Process of Megathrust Earthquake of magnitude 9

Hiroyuki Kikuchi[1]*

[1]Seismic Lab, 307, 12-1, 2-Chome, Wakamiya, Okegawa-shi, Saitama 363-0022, Japan

Key Points:

- Weak background vibration signals are binarized without losing Fourier spectral characteristics
- Thermodynamic state of ground motion is defined by the binarized signal
- State transition rate matrix and entropy production rate are evaluated from the thermodynamic states

*307, 12-1, 2-Chome, Wakamiya, Okegawa-shi, Saitama 363-0022, Japan

Corresponding author: Hiroyuki Kikuchi, hkikuchi@kkh.biglobe.ne.jp

Abstract

Sharp decrease of entropy production rate (EPR) is observed in the process of the Great East Japan Earthquake (GEJE) of magnitude 9. The EPR, a thermodynamic property of a fluctuating system, is calculated from the binarized velocity deviation of the background vibration. The background signal of the GEJE process includes a micron / second scale velocity signal that exhibits the dominant frequency of 1 Hz to 10 Hz in the Fourier amplitude spectrum. Paying attention to the negative curvature of the spectrum in the frequency range, we define α-tremor as the degree of negative curvature of the spectrum in the frequency range from 2.97 Hz to 9.80 Hz. The positive and non-positive α-tremor represent an arbitral weak velocity signal. The α-tremor has been shown to be invariant in binarizing the velocity fluctuation signal. Therefore, the binarized velocity and the raw velocity signal are equivalent as long as the background vibration is considered as the α-tremor fluctuation. The binarized velocity signal is divided into sets with 10 data, and the vibration state is defined for each set considering the degree of dispersion of the 10 signals. Then the transition rate from one state to the other is calculated, followed by the EPR calculation. The EPR is evaluated for ground vibration data acquired every 0.05 seconds from 2008 to 2014 at the seismic station 188 km away from the epicenter of GEJE which occurred in 2011.

1 Introduction

Strong earthquakes are a major concern in disaster management, and various measures are being taken for strong earthquakes. Earthquake Early Warning system in Japan warns people when an earthquake of 5 or greater is expected on the Japan seismic scale. When an earthquake is detected, the system analyzes the data captured by seismographs near the epicenter to estimate the epicenter, the magnitude of the earthquake and the seismic intensity. The estimated information is quickly released so that people can move to safe places or evacuate from dangerous places before strong surface waves arrive. Regarding building regulations, the seismic standards of the Building Standard Law in Japan require minor damage in medium-scale earthquakes with a seismic intensity of 5 or greater, and no collapses in large-scale earthquakes with a seismic intensity of 6 to 7.

On the other hand, earthquakes generally last less than a minute, and the dominant state of ground motion is seismically silent. Therefore, in order to understand the seismic process, it is necessary to investigate the silent state. Nonvolcanic tremor is one of the notable discoveries regarding the silent state. Obara investigated the seismically silent period in southwest Japan and identified the nonvolcanic tremor, the weak but noticeable signal with typical frequency range from 1 Hz to 10 Hz (Obara, 2002). Obara discussed that tremor with a long duration time is possibly caused by a chain reaction of small fractures induced by fluid. In 2003, Rogers and Dragert related tremors to ground slip events. Tremor activity accompanied by a slip event was observed approximately every 12 months for 6 consecutive years at Cascadia subduction zone interface (Rogers & Dragert, 2003). Regarding the mechanism of the long duration tremor, Peng and Chao observed the tremor induced by an earthquake and discussed that tremor occurred as a simple frictional response to the driving force (Peng & Chao, 2008).

This study focuses on the velocity signal of weak background vibrations in the silent state, and represents the background signal by α-tremors defined in a frequency range similar to that of tremors. Then, the invariance of α-tremor in the binarization of the velocity signal is shown. The binarized velocity and the raw velocity signal are considered as equivalent as long as the background vibration is considered as a α-tremor fluctuation. Following the velocity binarization, the vibrational states are defined, the stochastic dynamics of transitions of the state in a Markov process are described by the master equation, and entropy production rate (EPR) is calculated. Finally, the ERR is evaluated at the seismic station KSN, 188 km from the GEJE epicenter.

2 Observation of background signals

Ground vibration velocity data acquired every 0.05 seconds at the seismic station KSN is downloaded in chronological order from the web site of F-net, broadband seismograph network of National Research Institute for Earth Science and Disaster Resilience (NIED, 2019). The data is converted to piecewise deviation. Each section consists of 10 velocity data, and the piecewise deviation is the difference between the velocity within the section and the average velocity within the section. The piecewise deviation fluctuates around zero, and its squared average is the dispersion in statistics. The piecewise deviation data is divided into blocks of 1024 data, which corresponds to the data acquisition time of 51 seconds, and the Fourier amplitude of each block is calculated. The Fast Fourier Transform (FFT) algorithm is applied with no overlap, and no filtering. The upper bound of the frequency domain is 10Hz, which is half the data acquisition frequency. The lower bound is 0.02 Hz which is determined by the block size 1024. Therefore, the FFT with the sampling frequency of 20Hz and the block size of 1024 is equivalent to an FFT with a 0.02-10 Hz bandpass filter.

Fig. 1 shows a comparison of the velocities and spectrograms in the up-down (UD), north-south (NS), and east-west (EW) direction. The velocity data was acquired at KSN every 0.05 seconds from Mar. 3, 2011 to March 11, 2011. The period includes the magnitude 9 Great East Japan Earthquake (GEJE) occurred at 14:46 on March 11, 2011. In the spectrogram range from 1 Hz to 10 Hz, there are noticeable signals shown as the vertical brown lines. In the quiet period before the earthquake of magnitude 7.3, the timing of the vertical brown lines in the spectrograms (Fig. 2 (a4), (b2), and (c2)) respectively matches the timing of the wave clusters which have larger amplitude than surroundings (Fig. (a3), (b1), and (c1)). Since the UD component contains greater number of vertical brown lines than the other components, we focus on the UD component in the later sections.

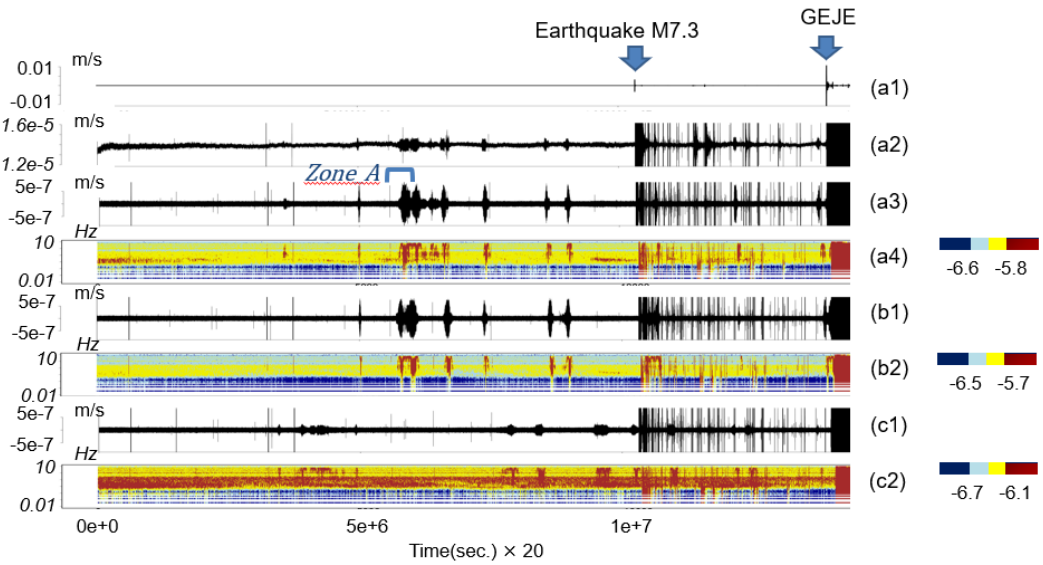

Figure 1: Background signals at KSN during March 3, 2011 to March 11,2011 period . (a1) Ground velocity (m/s) in UD direction. (a2) Magnified plot of (a1). (a3) Piecewise deviation of (a2). (a4) Spectrogram of (a3). (b1) Piecewise velocity deviation in NS direction. (b2) Spectrogram of (b1). (c1) Piecewise velocity deviation in EW direction. (c2) Spectrogram of (c1).

The third brown line in Fig. 1 (a4), which corresponds to the velocity deviation in Zone_A in Fig. 1 (a3), constructs a finer spectrogram structure. Fig. 2 shows the details of the Zone_A of 12500 second duration. The velocity deviation and its spectrogram are shown in Fig. 2 (a) and 2 (b), respectively. Fourier amplitude spectrum and its 10 moving averages are respectively indicated by the black and red lines in the Log10-Log10 plots of Fig. 2 (c1) to 2 (c6). The spectrogram is plotted from the 10 moving averages. The velocity deviations in Fig. 2 (d1) to 2 (d6) are the source data for the amplitude spectrum. The number below the velocity deviation graph indicates the time interval (seconds x 20). The velocity deviations are extracted from the beginning, center, end, and their intermediates of the period shown in Fig. 2 (a), and are chronologically exhibited from left to right. The first and last amplitude spectra show small negative curvatures in the range 1 Hz to 10 Hz (Fig. 2 (c1) and 2 (c6)). The rest of the spectra show large values and negative curvatures in the range from 1 Hz to 10 Hz (Fig. 2 (c2) to 2 (c5)). The curvature widens in the center of the zone and narrows in the rest of the zone. The amplitude of the velocity deviation is small at the beginning and end, and large in the central zone.

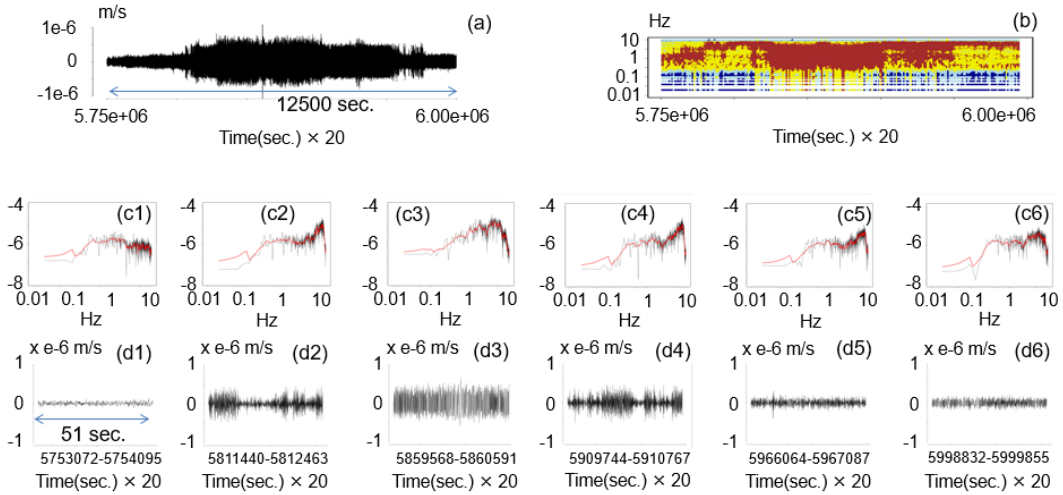

Figure 2: Fine structure of the signal in the Zone_A in Figure 1 (a3). (a) UD velocity deviation (m/s). (b) Spectrogram of (a). (c1)-(c6) Fourier amplitude spectrum excerpted from (b). (d1)-(d6) UD velocity deviation, the source data for (c1)-(c6).

3 Definition of α-tremor

The curvature of the Fourier amplitude spectrum is defined as the ratio of $P_{ni}-P_i$ to $|P_2-P_1|$ in Fig. 3 (a), where P_i is the point of the (frequency, spectrum) coordinate system. The frequency of P_1 and P_2 are 2.97 Hz and 9.8 Hz, which correspond to the 152th and 502th point on the frequency axis, respectively. The average of the spectrum value of the nearest 5 points are assigned as the spectrum value for the P_1 and P_2. P_i is a point in the 2.97-9.8 Hz range. P_{ni} is determined so that the line from P_i to P_{ni} is perpendicular to the line connecting P_1 and P_2. If the spectrum value of P_i is greater than that of P_{ni}, the curvature is negative. Otherwise, the curvature is non-negative. The curvature is independent of the scale change since the line length in log10 plot is invariant to the scalar multiplication of the coordinate values.

We define α-tremor as the product of -1 and the curvature of which absolute value is greater than the absolute value of other curvatures in the frequency range of 2.97 to 9.8 Hz (Fig. 3 (a)). An arbitrary ground velocity signal is classified as either positive α-tremor or non-positive α-tremor.

The α-tremor for the velocity data acquired at KSN during March 03, 2011 to March 11, 2011 is exhibited in Fig. 3 (b). As expected, the positive peak of the α-tremor appears at a timing similar to the brown line in Fig. 1 (a4).

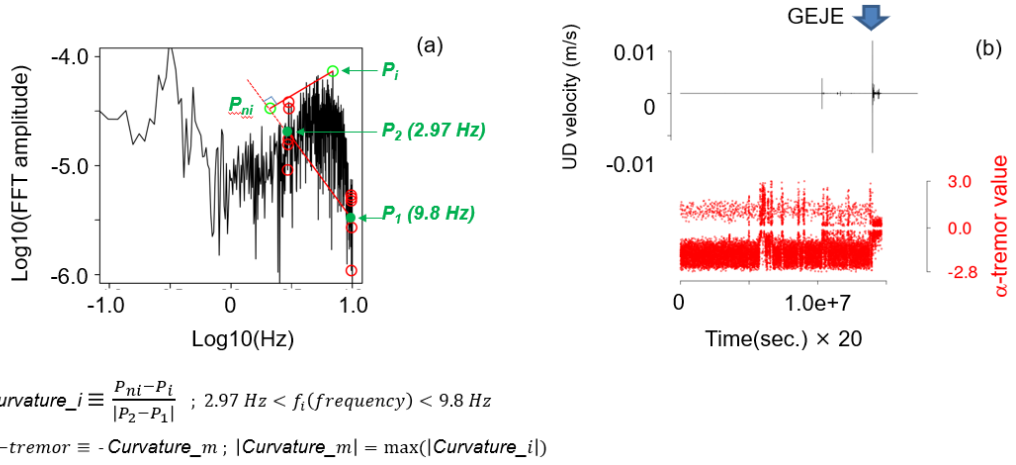

$$Curvature\_i \equiv \frac{P_{ni}-P_i}{|P_2-P_1|} \;;\; 2.97\ Hz < f_i(frequency) < 9.8\ Hz$$

$$\alpha\text{-}tremor \equiv -Curvature\_m \;;\; |Curvature\_m| = \max(|Curvature\_i|)$$

Figure 3: Definition of α-tremor. (a) Definition of spectrum curvature and α-tremor. (b) α-tremor calculated for the UD velocity data of $Fig.1(a1)$.

It should be noted that the piecewise velocity deviation is equivalent to the raw velocity data in evaluating the α-tremor. Fig. 4 (a) compares the Fourier amplitude spectrum of the velocity deviation data to the amplitude spectrum of the raw velocity data. In the range of 2.97 Hz to 9.8 Hz, the amplitude spectrum of the deviation velocity (black line) matches the spectrum of the raw data (green line) by 80%. Therefore, we may select either the piecewise deviation velocity data or the raw velocity data to obtain a unique amplitude spectrum in the range 2.97 Hz to 9.8 Hz. The α-tremor in the subsequent sections is calculated from the raw velocity data for convenience. The orange and red lines in Fig. 4 (a) are the 10-moving averages of the black and green lines, respectively. The source data of the spectrum, which are the velocity deviation and velocity acquired at KSN during the period from March 1, 2012 to March 10, 2012, are shown in Fig. 4 (b) and 4 (c), respectively.

4 Binarization of velocity deviation data

The velocity deviation data is binarizable without losing the α-tremor property. In Fig. 5, the Fourier amplitude spectrum and spectrogram calculated from the velocity deviation are compared to those calculated from the binarized velocity deviation. Fig. 5 (a1) and 5 (b1) shows the binarization procedure. If each velocity deviation data in Fig. 5 (a1) is greater than the mean of the data set under consideration, the deviation data is converted to 1, otherwise the deviation data is converted to 0. The binarized data can be expressed as the time sequence of 0 and 1 as shown in Fig. 5 (b1). The clear negative curvature in the frequency range 1 Hz to 10 Hz, shown in both the Fourier spectrum of the velocity deviation and the binarized data, implies that the α-tremor is pre-

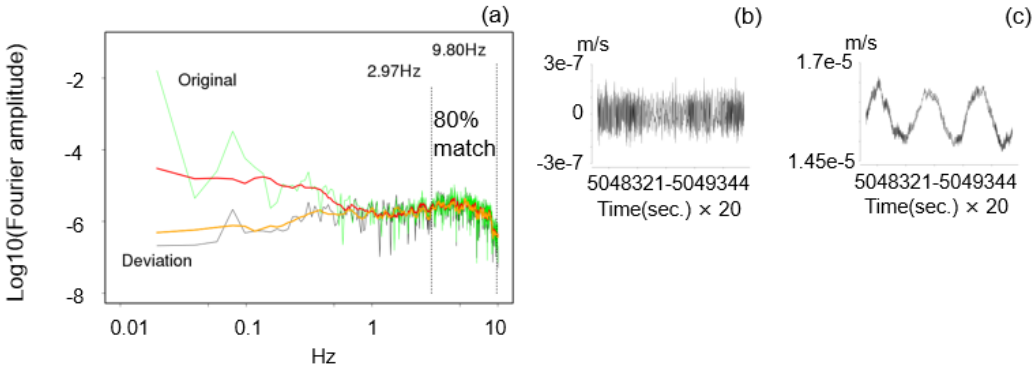

Figure 4: Comparison of velocity deviation spectrum and velocity spectrum, which have negative curvatures. Spectrums of background signals recorded at KSN during the period from March 1, 2012 to March 10, 2012. (a) Fourier amplitude spectrum of velocity in the UD direction, and spectrum of deviation velocity. (b) UD velocity deviation data. (c) UD velocity data.

served in the binarization (Fig. 5 (a2) and (b2)). Fig. 5 (a3) is the Fourier amplitude spectrogram duplicated from Fig. 2 (b), of which source data is the velocity deviation shown in Fig. 2 (a). The source data is binarized and its spectrogram is calculated as shown in Fig. 5 (b3). The qualitative similarity between the spectrogram of the binarized data and the spectrogram of the source data suggests that the α-tremor is preserved in the binarization (Fig. 5 (a3) and (b3)). Therefore, the binarized velocity and velocity deviation are equivalent as long as the background vibration is considered as a α-tremor fluctuation.

5 Definition of background vibration state

Since the α-tremor is conserved in the binarization of the velocity signal, the essential of the ground motion is the distribution of the signal rather than the shape of the signal. Therefore, it is reasonable to define the ground vibration state in a specified time interval by counting the cluster of 1 in the interval of the binarized velocity. In defining the vibration state, the binarized velocity sequence (Fig. 6 (a)) is divided into blocks with 10 data points, and the number of clusters of "1" is counted in each block. In order to preserve the total number of the cluster, the rule shown in Fig. 6 is applied. In the 10-data block, we scan the cell from left to right and count one if the sequence of "10" is found. At the end of the scan, at the 10th data point, we count one only if the 11th data point is "0" (Fig. 6 (b)). The counting rule restricts the maximum number of clusters in a block to five, and defines five vibrational states s_1, s_2, s_3, s_4 and s_5, each containing 1, 2, 3, 4, and 5 clusters (Fig. 6 (c1)- 6 (c5)).

6 Thermodynamics of the ground vibration

Fig. 7 (a) shows the first 100 data of the binarized velocity deviation data of Fig. 5 (b1). The 10 data in each row of Fig. 7 (b) are the binarized velocity deviation data splitted from Fig. 7 (a), and constitute the vibration state with a time interval of 0.5 seconds. In general, the vibration state shows a different pattern of binary sequence for each row and contains a different number of clusters for each row (Fig. 7 (c)). Since each row corresponds to a different time, the state of background vibration fluctuates over time.

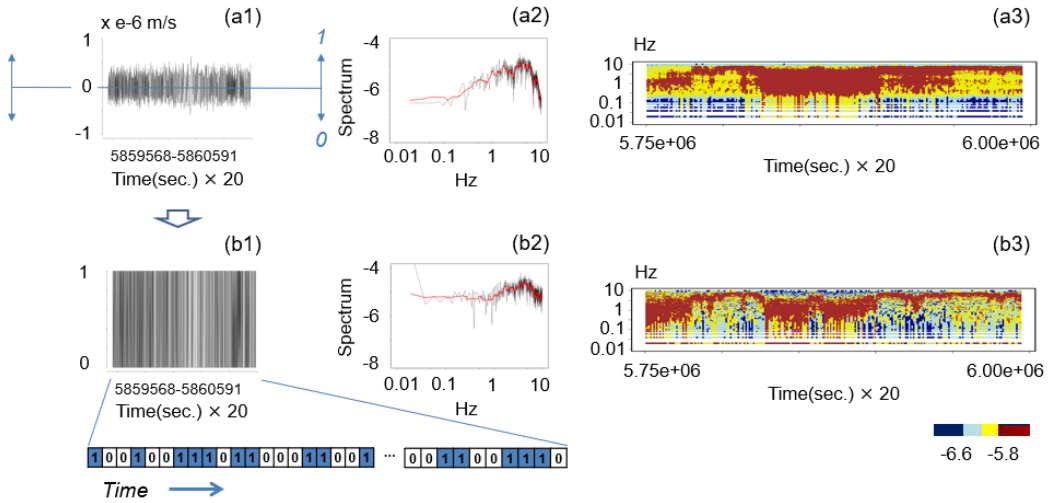

Figure 5: Binarization of velocity deviation. (a1) Velocity deviation duplicated from *Fig*.2(*d*3). (a2) Fourier amplitude spectrum of (a1). Duplicate of *Fig*.2(*c*3). (a3) Fourier amplitude spectrogram of the velocity deviation recorded at KSN during 5.75e6 to 5.6e6 (sec x 20). The time origin is 00:00 on March 3, 2011. Duplicate of *Fig*.2(*b*). (b1) Binarization result of (a1). (b2) Fourier amplitude spectrum of (b1). (b3) Fourier amplitude spectrogram of the binarized velocity deviation recorded at KSN during 5.75e6 to 5.6e6 (sec x 20). The time origin is 00:00 on March 3, 2011. Compare with (a3).

The time series of the number of clusters in Fig. 7 (c) shows the history of the state transitions. Since the number of clusters in a state is defined as a state index, the square brackets that make up the pair of two numbers indicate that the state of the number in the lower row has transitioned to the state of the number in the upper row. The transition rate matrix W_{ij} defines the total number of transitions from i-state to j-state so that the W_{ij} count is incremented by 1 when a transition from i-state to j-state occurs (Fig. 7 (d)). The result of the W_{ij} counting for the 100 data is shown in Fig. 7 (e). Fig. 7 (f) shows the probability density vector, of which component p_i is the total number of i-state.

The state of background vibration, which fluctuate over time, implies that the state is non-equilibrium. It is known that the thermodynamics of a fluctuating nonequilibrium system are described by the master equation (Eq. (1)), and the entropy production rate (Eq. (2)) which is similar to the entropy of the second law of thermodynamics of equilibrium systems (Haitao, Y. & Jiulin, D., 2014).

$$\frac{dp_i}{dt} = \sum_{j=1}^{n} J_{ij}(t) \tag{1}$$

$$J_{ij}(t) = W_{ij}(t)p_j(t) - W_{ji}(t)p_i(t)$$

$$F_{ij}(t) = ln\frac{W_{ij}(t)p_j(t)}{W_{ji}(t)p_i(t)}$$

$$\sigma(t) = \frac{1}{2}\sum_{i=1}^{n}\sum_{j=1}^{n} J_{ij}(t)F_{ij}(t) \tag{2}$$

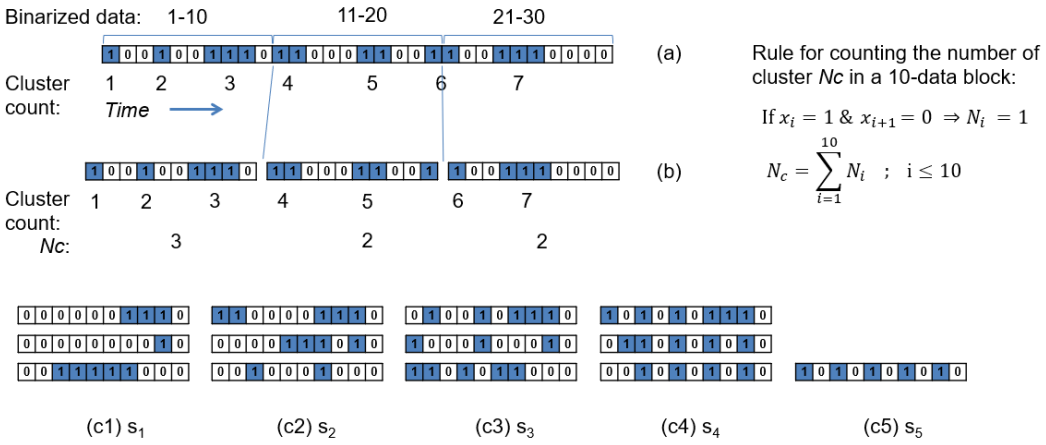

Figure 6: Definition of background vibration state. (a) Sequence of binarized velocity deviations and counts of "1" clusters. (b) Blocks with 10 data points divided from the sequence in (a), and counts of "1" clusters. (c1)-(c5) Examples of the background vibration state s_1, s_2, s_3, s_4, and s_5, each containing 1, 2, 3, 4, and 5 clusters.

where W_{ij} and p_i are coherent with those in Fig. 7. J_{ij} and F_{ij} are called the flow from i-state to j-state and thermodynamic force, respectively.

Fig. 8 shows EPR, the Fourier amplitude spectrum, W_{ij} contour plot, and the vibration states in the first 10 time steps. These are calculated from the binarized data of the velocity deviation in Fig. 2 (d1) -2 (d6). Small positive α-tremors, or small negative curvatures in the spectrum from 2.97 to 9.8 Hz, tend to be accompanied by a small EPR (Fig. 8 (a1) and 8 (a6)).

7 Thermodynamics in the process of GEJE

EPR is evaluated for the UD velocity data acquired at KSN every 0.05 seconds from January 1, 2008 to December 30, 2014. The EPR is calculated every 10 days, and the 3-months moving average of the EPR is plotted in Fig. 9 (b). EPR sharply decreases from January 1, 2008 to the timing of GEJE on March 11, 2011. For approximately 1.5 years after GEJE, EPR remains low and then recovers approximately 50 %.

The changes in EPR in the GEJE process are compared to the time evolution of α-tremor evaluated for the velocity data acquired at KSN every 0.05 seconds from January 1, 2006 to December 30, 2018. Fig. 9 (c) shows positive α-tremor and the timing of earthquakes with seismic intensities greater than 4, which occurred during the period. For GEJE of magnitude 9, seismic intensity 6 was recorded at Kesennuma City, which is the observation point of seismic intensity approximately 10km from KSN (filled blue rectangle on the map in Fig. 9 (a)). The white circle and red $\oplus$ on the map are the location of the seismic station KSN and the epicenter of the earthquake, respectively. The table in Fig. 9 includes the identifiers of earthquakes, date, magnitude, seismic intensity, and the epicenter of the earthquakes searched on the website of the Japan Meteorological Agency of Ministry of Land, Infrastructure, Transport and Tourism (JMA-1, 2019). The search conditions are the seismic intensity greater than 4, the location of observing the seismic intensity, and the time period for search.

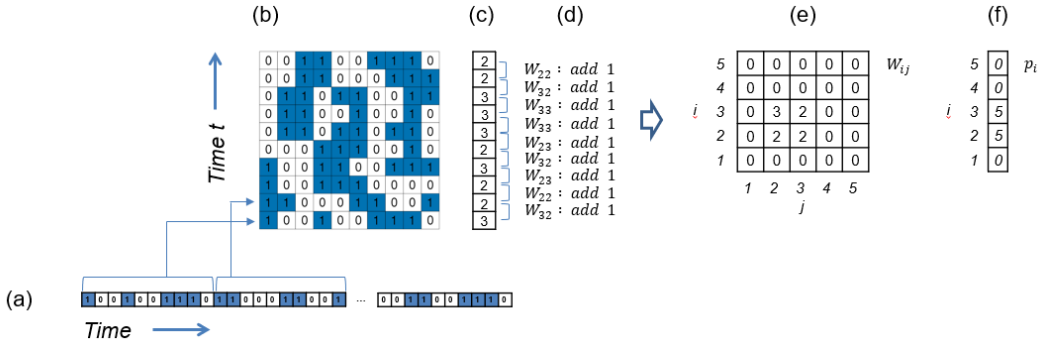

Figure 7: Transition rate matrix and probability density of state. (a) The first 100 data of the binarized velocity deviation data of $Fig.5(b1)$. (b) A pile of blocks containing 10 data points divided from (a). (c) The number of clusters in the block, or the index "i" of the vibration state s_i. Chronological transition sequence from the lower state s_i to the upper state s_j. (d) The procedure for calculating W_{ij}, which is a component of the transition rate matrix. (e) W_{ij} calculated for (c). (f) Probability density distribution of states in the 100 data in (c). The numbers are not normalized. p_i is the total number of the states s_i in the 100 data.

Several α-tremor peaks are observed at KSN before and after GEJE in Fig. 9 (c). Since the timing of the α-tremor peaks do not match the timing of the earthquakes A and D, those α-tremors are probably not induced by earthquakes. It should be noted that density of the data point of the weak positive α-tremor below 0 in the log10 plot is discontinuously increased after GEJE. The small EPR after GEJE (Fig. 9 (b)) and the high density of the small positive α-tremor after GEJE (Fig. 9 (c)) is coherent with the previous discussions on Fig. 8 that small positive α-tremor implies small EPR.

8 Conclusions

In order to analyze the thermodynamic changes in the vibration state of the ground during the seismic process of GEJE, EPR has been calculated from the state transition rate matrix and density distribution of the vibration state defined by the binarized velocity deviation of the weak background vibration of the ground. The binarized data is equivalent to the raw velocity data, assuming that the background vibration is represented by the α-tremor. It is found that EPR decreases sharply from January 1, 2008 to the timing of GEJE on March 11, 2011, then remains low for approximately 1.5 years and then recovers by approximately 50 %. The low level of the EPR after GEJE probably due to the dense distribution of data points of the weak positive α-tremor after GEJE.

Acknowledgments

Data is publicly available through National Research Institute for Earth Science and Disaster Resilience, National Research and Development Corporation under Ministry of Education, Culture, Sports, Science and Technology. F-Net (Broadband seismograph network) data base. http://www.fnet.bosai.go.jp/top.php?LANG=en.

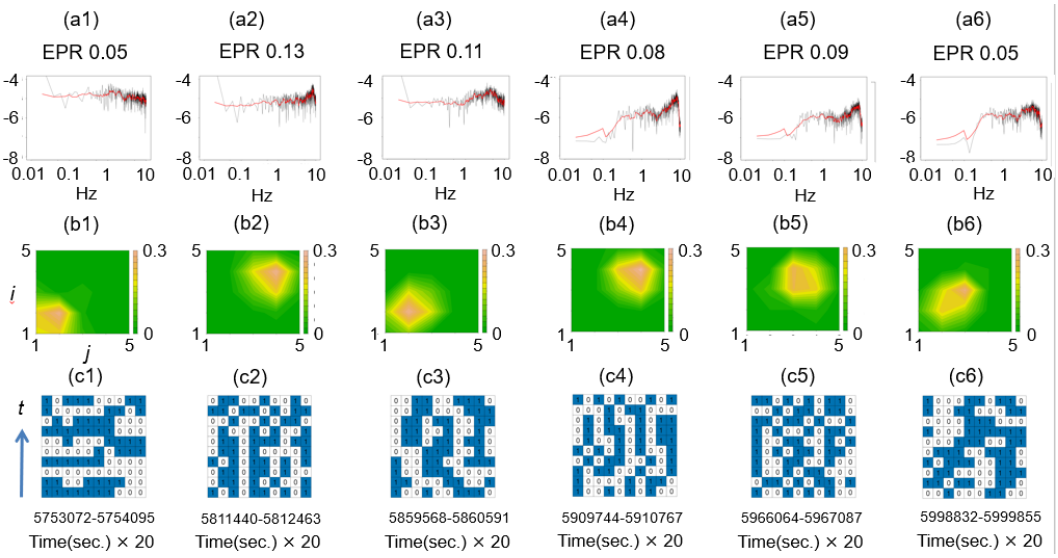

Figure 8: Thermodynamics of the background signal in the Zone_A in $Fig.1(a3)$. Corresponds to $Fig.2$. (a1)-(a6) EPR and Fourier amplitude spectrum calculated from the binarized data of the velocity deviation in $Fig.2(d1) - 2(d6)$. (b1)-(b6) W_{ij} contour plot. (c1)-(c6) Vibration states in the first 10 time steps.

References

Obara, K. (2002). Nonvolcanic Deep Tremor Associated with Subduction in Southwest Japan. Science 31 May 2002: Vol. 296, Issue 5573, pp. 1679-1681. DOI: 10.1126/science.1070378

Rogers, G. & Dragert, H. (2003). Episodic Tremor and Slip on the Cascadia Subduction Zone: The Chatter of Silent Slip. Science 20 Jun 2003: Vol. 300, Issue 5627, pp. 1942-1943. DOI: 10.1126/science.1084783

Peng, Z. & Chao, K. (2008), Non-volcanic tremor beneath the Central Range in Taiwan triggered by the 2001Mw 7.8 Kunlun earthquake. Geophys. J. Int. (2008) 175, 825-829 doi: 10.1111/j.1365-246X.2008.03886.x

NIED (2019). National Research Institute for Earth Science and Disaster Resilience, National Research and Development Corporation under Ministry of Education, Culture, Sports, Science and Technology. F-Net (Broadband seismograph network) data base. DOI: 10.17598/nied.0005. http://www.fnet.bosai.go.jp/top.php?LANG=en

Haitao, Y. & Jiulin, D. (2014), Entropy Production Rate of Non-equilibrium Systems from the Fokker-Planck Equation. Braz J Phys 44, 410-414 (2014). https://doi.org/10.1007/s13538-014-0234-6

JMA-1. (2019). Japan Meteorological Agency under Ministry of Land, Infrastructure, Transport and Tourism. Seismic intensity database search. https://www.data.jma.go.jp/svd/eqdb/data/shindo/index.php

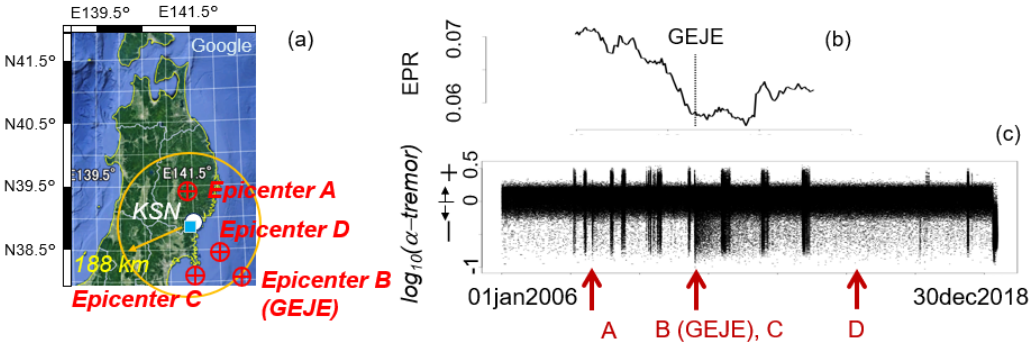

ID	Date	Magnitude	Seismic Intensity	Latitude	Longitude	Depth(km)
A	Jul. 24, 2008	6.8	5	$39.43N$	$141.38E$	108
B	Mar. 11, 2011	9	6	$38.06N$	$142.51E$	24
C	Apr. 07, 2011	7.2	5	$38.12N$	$141.55E$	66
D	May 13, 2015	6.8	5	$38.52N$	$142.09E$	46

Figure 9: Thermodynamics in the seismic process of GEJE. (a) Location of KSN, epicenter of the earthquake listed in the table, and measurement point of seismic intensity. (b) EPR. (c) Positive α-tremor.